Paleoceanography and Paleoclimatology

Supporting Information for

Early to Middle Miocene Astronomically-Paced Climate Dynamics in the Eastern Equatorial Atlantic

Bianca R. Spiering[1], Evi Wubben[1], Frederik J. Hilgen[1], and Appy Sluijs[1]

[1]Department of Earth Sciences, Faculty of Geosciences, Utrecht University, Utrecht, The Netherlands

Contents of this file

Introduction

This Supporting Information contains additional text, figures and a table that support the main text.

Text S1. Pre-MCO age model.

Alternative age models for the interval prior to the onset of the MCO (i.e., cores 26X and 27X) cannot be excluded. The pre-MCO age model presented in the main text is based on the calcareous nannofossil biostratigraphy and results in a hiatus of ~750 kyr (Figure 3; Wubben et al., 2023). The pronounced $\delta^{13}C$ minima that were recognized in the depth domain could also be correlated to younger ~100 kyr eccentricity maxima. An alternative age model resulting in more continuous sedimentation was presented by Wubben et al. (2023). Here, we present two other alternative age models.

Assuming continuous sedimentation, the pre-MCO interval would occur between ~17.6 and ~17 Ma (Figure S1a-b). In this option, the very weak ~100 kyr maximum around ~17 Ma might occur at the top of core 26X without any pronounced $\delta^{13}C$ minimum. The interval between the two pronounced $\delta^{13}C$ minima at ~270 and ~274 rmbsf now corresponds to a 400 kyr eccentricity minimum, while the generally low $\delta^{13}C$ values might suggest that it should correspond to a 400 kyr eccentricity maximum. Moreover, the $\delta^{13}C$ minimum at ~277 rmbsf is relatively weak, suggesting it should correspond to a 400 kyr eccentricity minimum instead of a maximum.

A particularity in the eccentricity solution in this time interval is the shoulder occurring at ~17.4 Ma. This shoulder is a weak ~100 kyr maximum that might not result in a pronounced $\delta^{13}C$ minimum. Therefore, considering a stable sedimentation rate, we would expect the presence of an interval where the distance between pronounced $\delta^{13}C$ minima is significantly larger. This now corresponds to the relatively large interval between $\delta^{13}C$ minima at ~270 and ~274 rmbsf.

We present a second alternative option in which the interval around the shoulder correlates to the interval with the largest distance between pronounced $\delta^{13}C$ minima, namely between $\delta^{13}C$ minima at ~262 and ~267 rmbsf (Figure S1c-d). In this option, the pre-MCO interval would occur between ~17.8 and ~17.2 Ma, with a hiatus of ~300 kyr at the onset of the MCO. The tuning of core 27X is the same as in the alternative option of Wubben et al. (2023). This age model fits well with the expectation of a 400 kyr maximum around ~270-274 Ma.

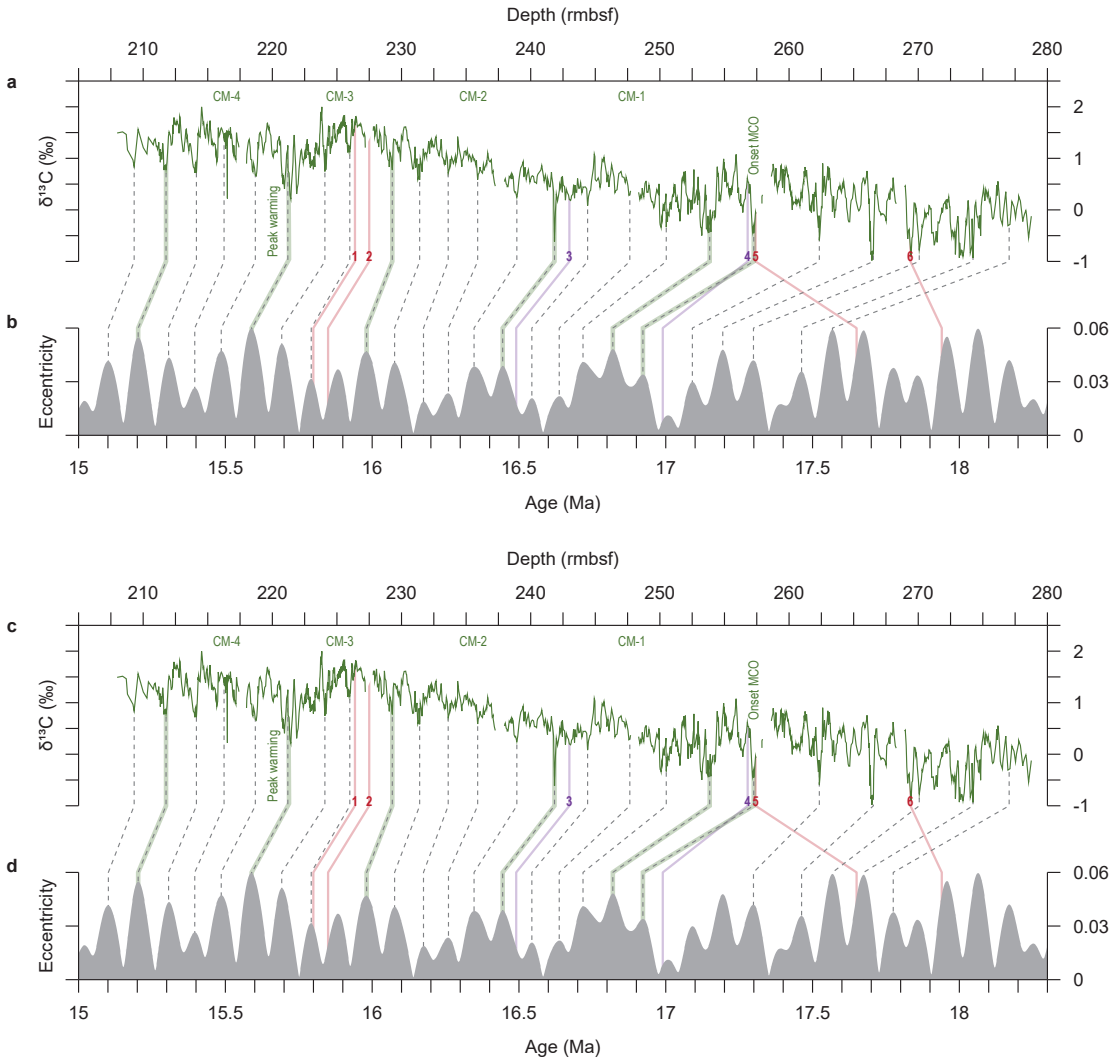

Figure S1. Alternative astronomical tuning of the pre-MCO with continuous sedimentation (**a-b**) and a ~300 kyr hiatus (**c-d**). Tie-points (dashed grey lines) connect pronounced $\delta^{13}C$ minima to eccentricity maxima (Laskar et al., 2004). Chemo- and biostratigraphic markers are indicated by the colored lines (see caption Figure 3).

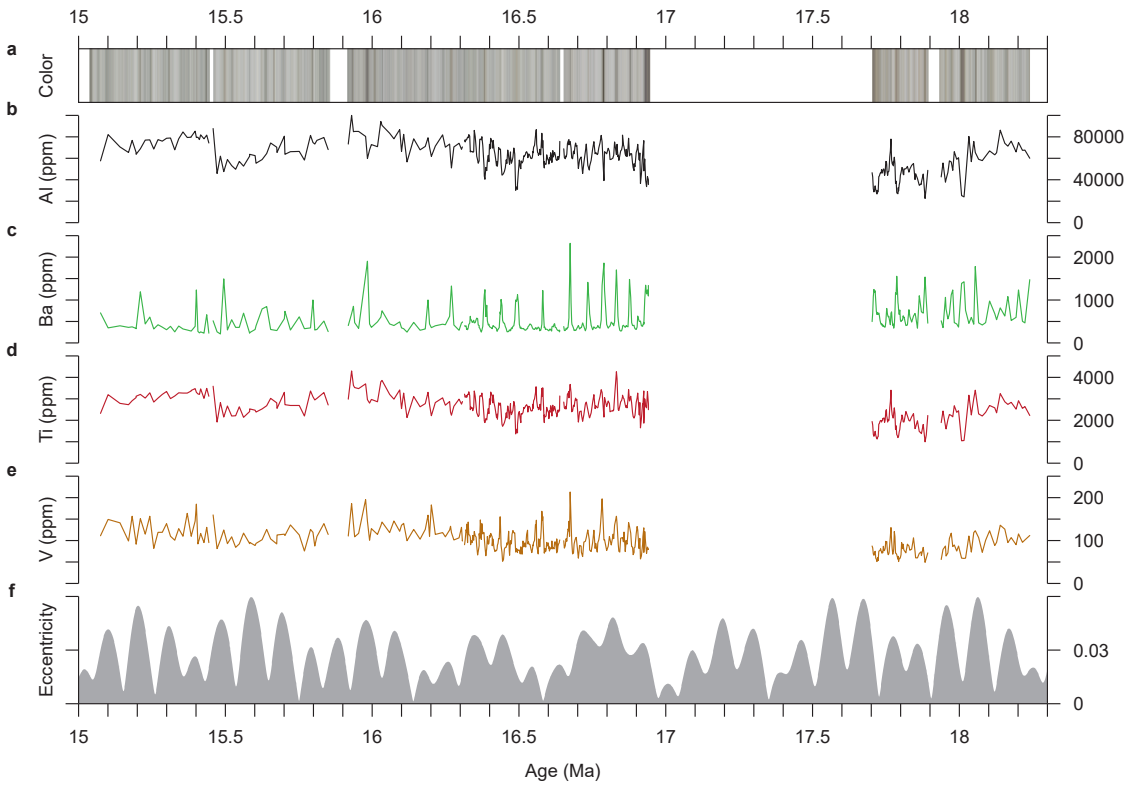

Figure S2. Overview of Early to Middle Miocene elemental concentrations from Site 959: (**a**) color, (**b**) Al, (**c**) Ba, (**d**) Ti, (**e**) V, and (**f**) the La2004 eccentricity solution (Laskar et al., 2004).

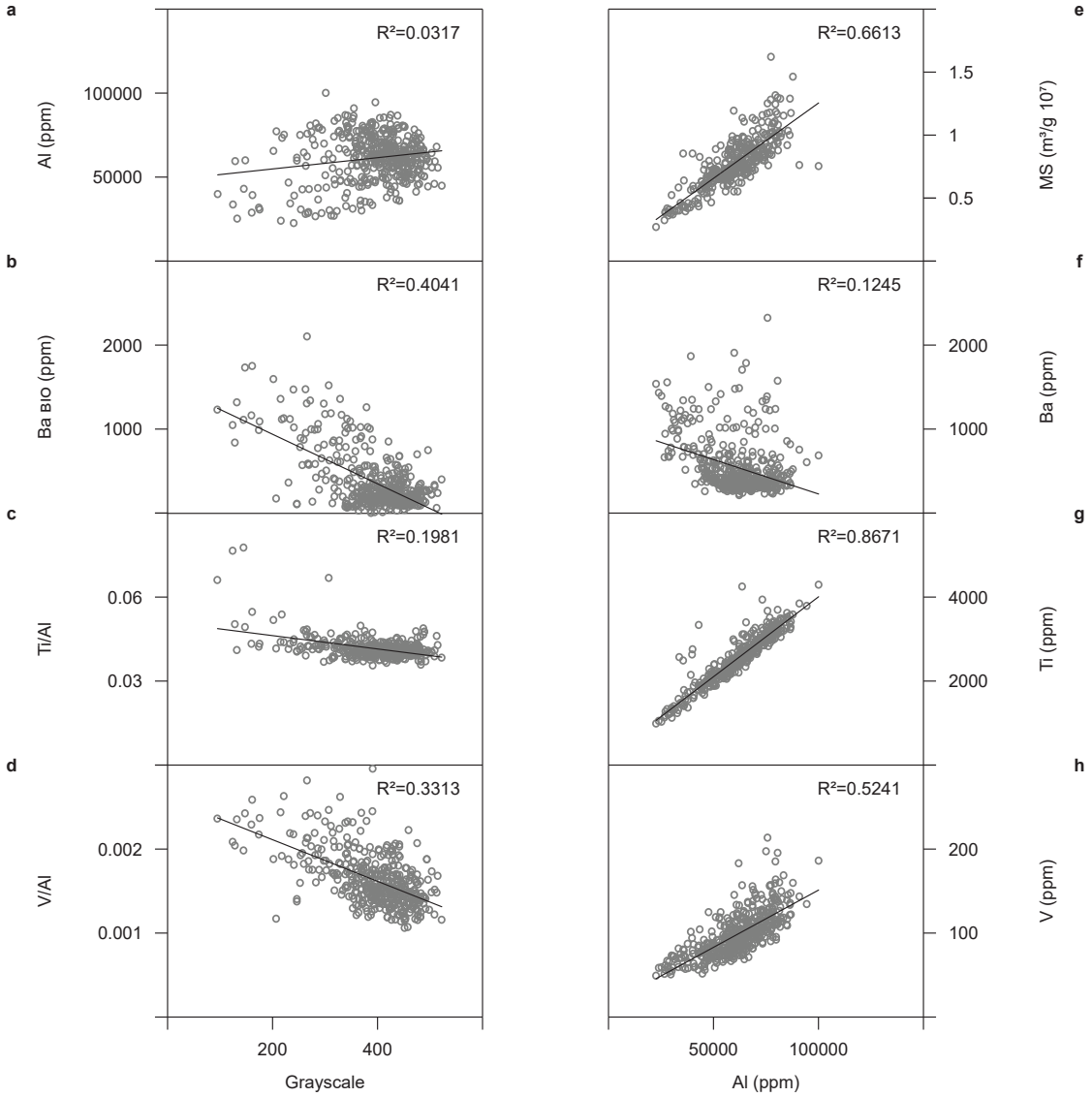

Figure S3. Scatter plots showing the relationship between Site 959 data. Grayscale is plotted against Al (**a**), Babio (**b**), Ti/Al (**c**), and V/Al (**d**). Al is plotted against MS (**e**), Ba (**f**), Ti (**g**), and V (**h**). Linear trendlines (solid black) and R-squared values are indicated.

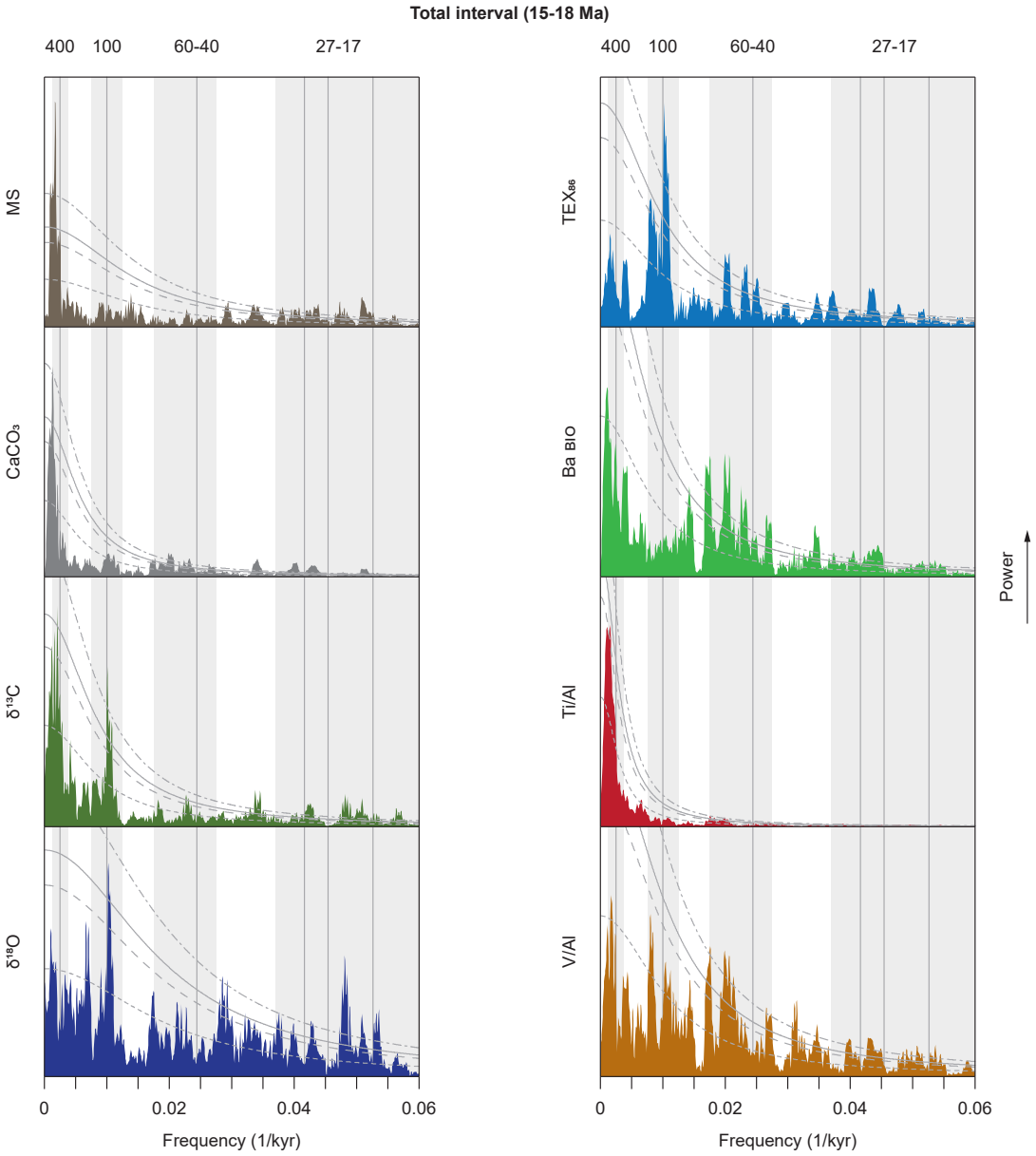

Figure S4. Power spectra of Site 959 proxy data for the total Early to Middle Miocene interval (18-15 Ma). A linear scale is used for both the x (frequency) and y (power) axes. AR1 fit, and 90%, 95%, and 99% confidence levels are indicated by the small dashed, large dashed, solid, small-large dashed gray lines, respectively. The gray bars indicate important frequency bands representing periodicities of ~400 kyr, ~100 kyr, ~60-40 kyr, and ~27-17 kyr. The vertical gray lines indicate exact periods of 400, 100, 41, 24, 22, 19 kyr.

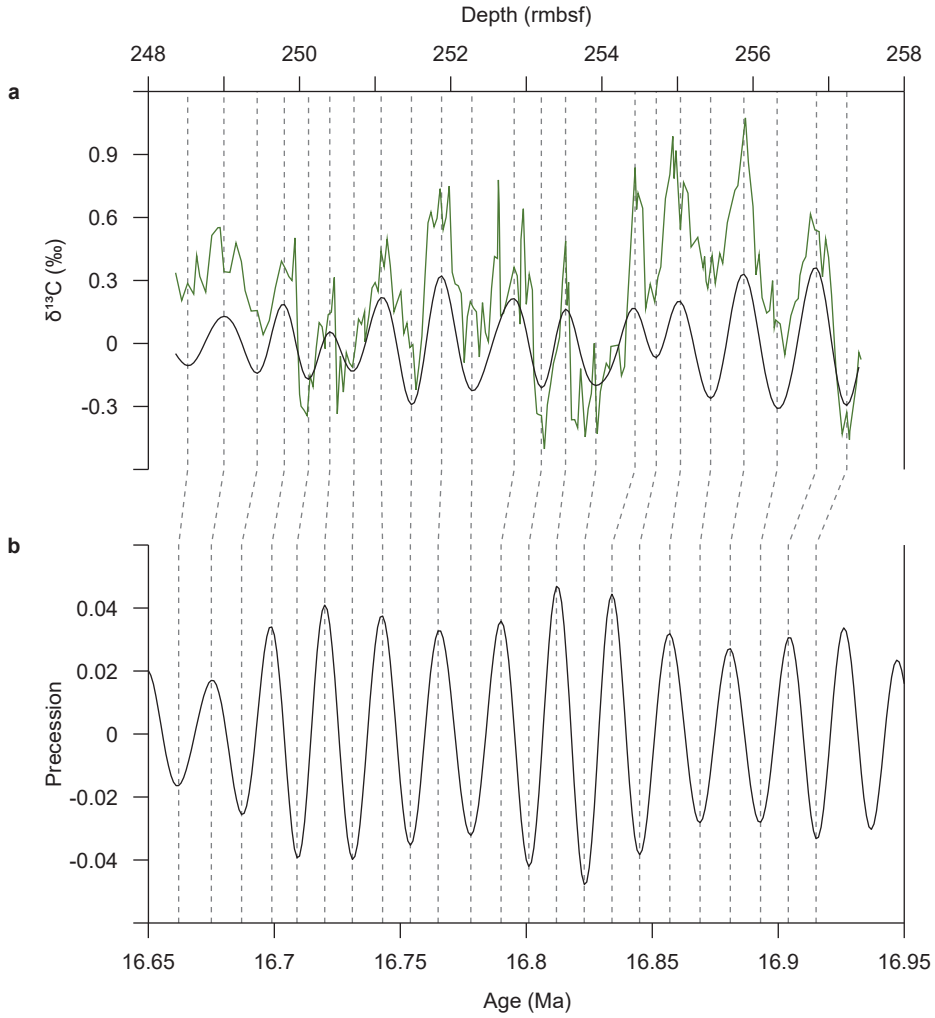

Figure S5. Tuning of the bulk carbonate $\delta^{13}C$ record of core 25X to precession. The $\delta^{13}C$ record (green) is plotted in the depth domain with its bandpass filter with a width of 0.63-1.75 1/m (black; **a**). Tie-points (dashed gray lines) connect minima and maxima of the $\delta^{13}C$ bandpass filter in the depth domain (**a**) to precession minima and maxima in the La2004 solution (Laskar et al., 2004, **b**).

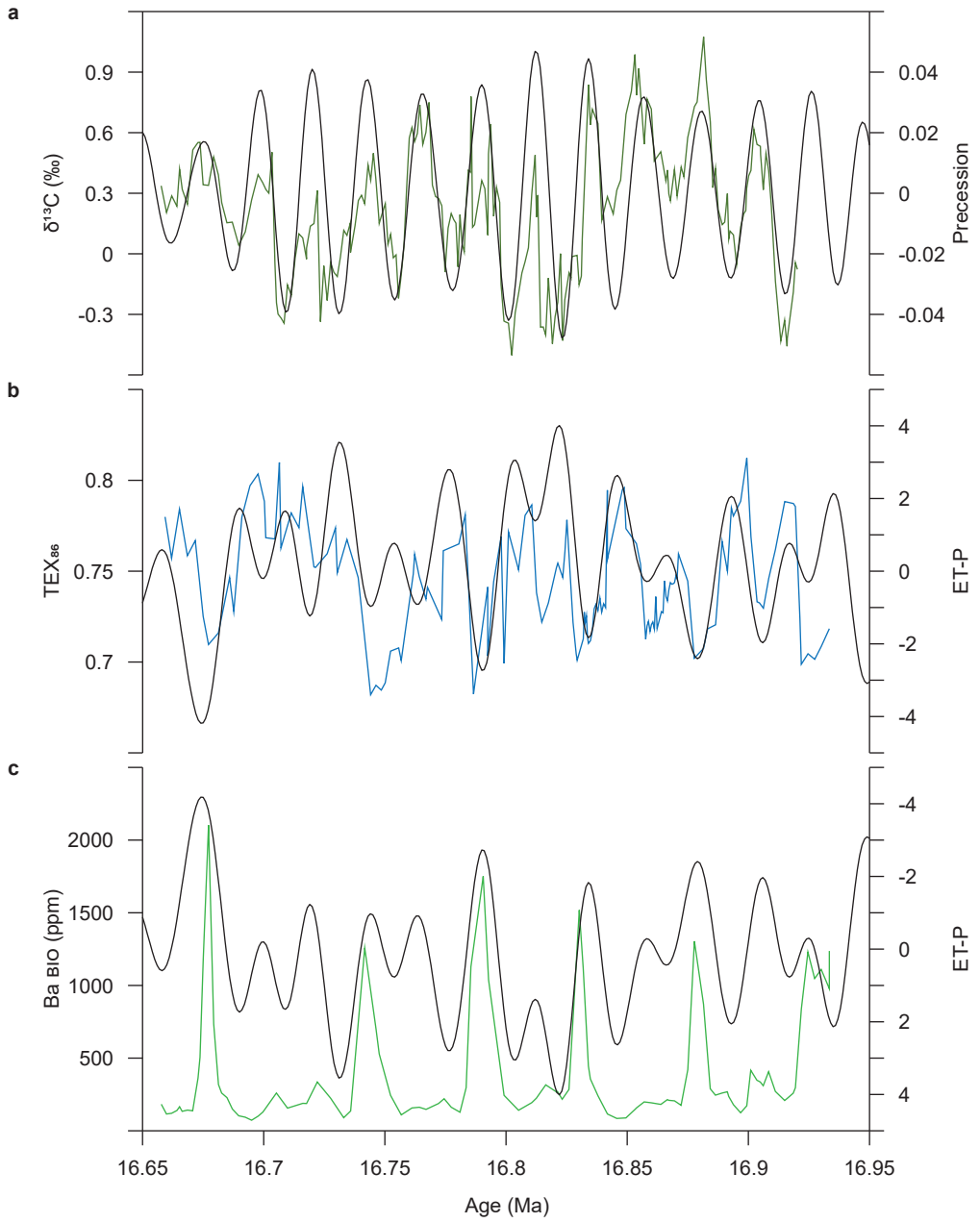

Figure S6. Precession-tuned proxy data of $\delta^{13}C$ (green; **a**), TEX_{86} (blue; **b**), and Ba_{bio} (green; **c**) compared to precession (black; **a**) and standardized eccentricity, tilt, and reversed-precession (ET-P) curve (black; **b-c**) of the La2004 solution (Laskar et al., 2004).

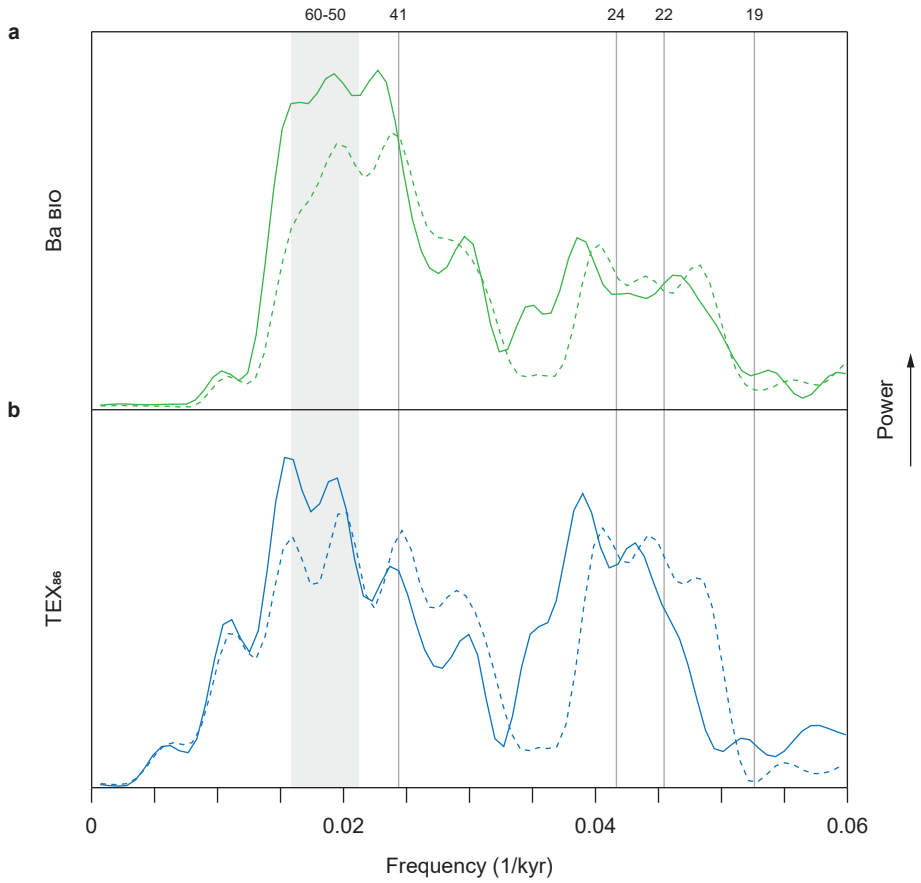

Figure S7. Power spectra of Ba_{bio} (**a**) and TEX_{86} (**b**) for the interval of core 25X (~16.65-16.95 Ma) using the eccentricity-tuned age model (solid lines) and the precession-tuned age model (dashed lines). A linear scale is used for both the x (frequency) and y (power) axes. The gray bar and vertical lines indicate important periodicities (in kyr).

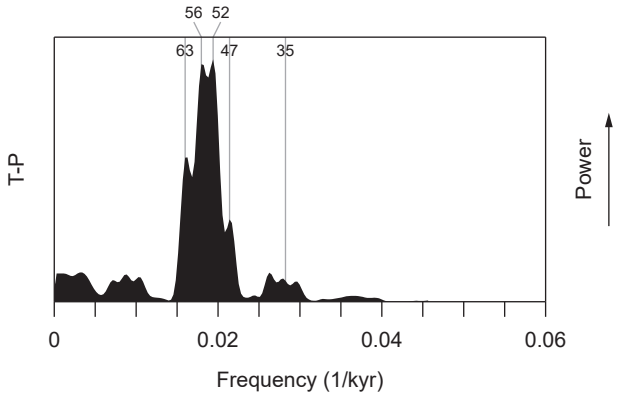

Figure S8. Power spectrum of the amplitude modulation of the standardized tilt and reversed-precession (T-P) curve for the interval 16.9-16.3 Ma. A linear scale is used for both the x (frequency) and y (power) axes. The vertical gray lines indicate periodicities (in kyr) of major peaks in the spectrum. The astronomical solution is derived from La2004 (Laskar et al., 2004).

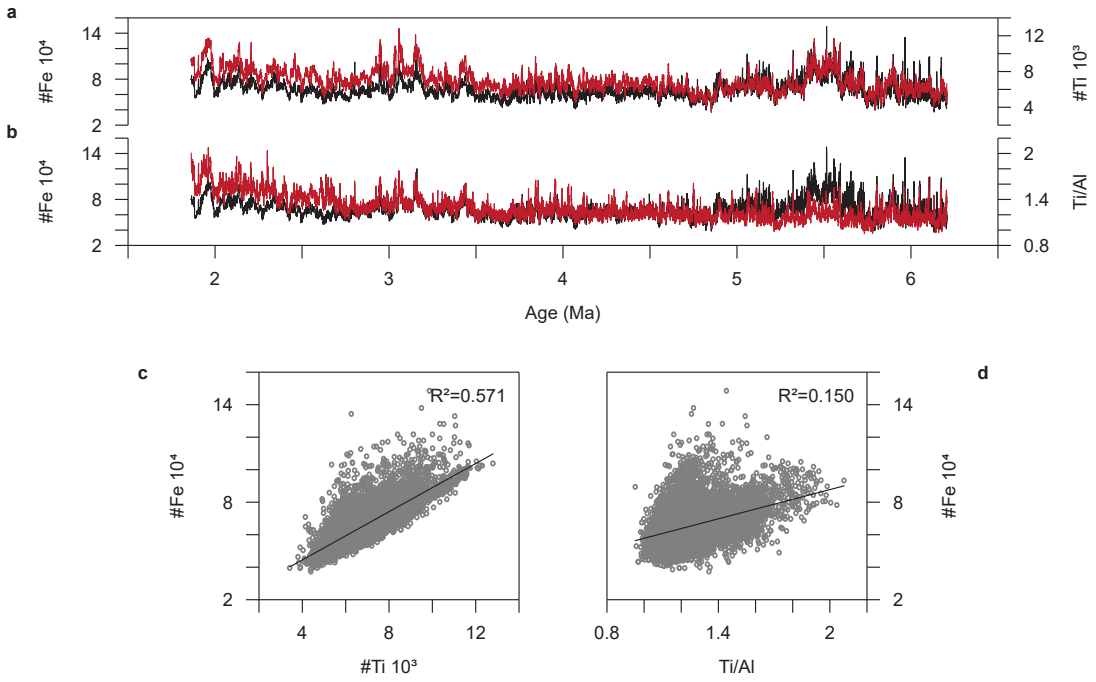

Figure S9. Fe intensity data compared to Ti intensity and Ti/Al data of Site 959 for the interval 2-6 Ma (Vallé et al., 2017). The Fe count record (black) is compared to Ti count (red; **a**) and Ti/Al (red; **b**). Scatter plots show the relationship between Fe count and Ti count (**c**), and Fe count and Ti/Al (**d**). Linear trendlines (solid black) and R-squared values are indicated.

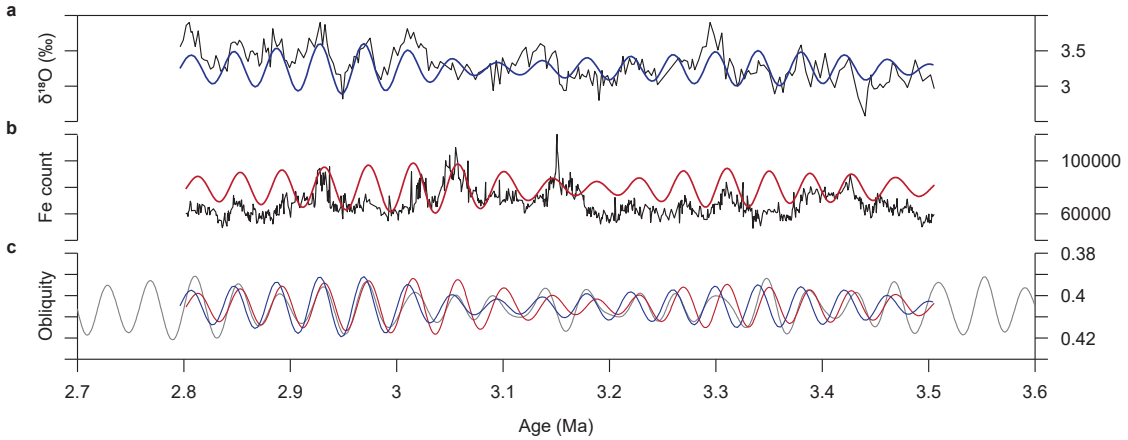

Figure S10. Benthic $\delta^{18}O$ (black; **a**) and Fe intensity data (black; **b**) of Site 959 for the 3.5-2.8 Ma interval. The data are derived from van der Weijst et al. (2020) and Vallé et al. (2017), respectively. Bandpass filters of ~41 kyr cyclicity in $\delta^{18}O$ (blue) and Fe (red) are compared to obliquity (gray; **c**) of the La2004 solution (Laskar et al., 2004). Data is plotted on the revised age model of van der Weijst et al. (2020). The following bandpass filter widths (in 1/kyr) were used: 0.021-0.028 for $\delta^{18}O$, and 0.021-0.028 for Fe.

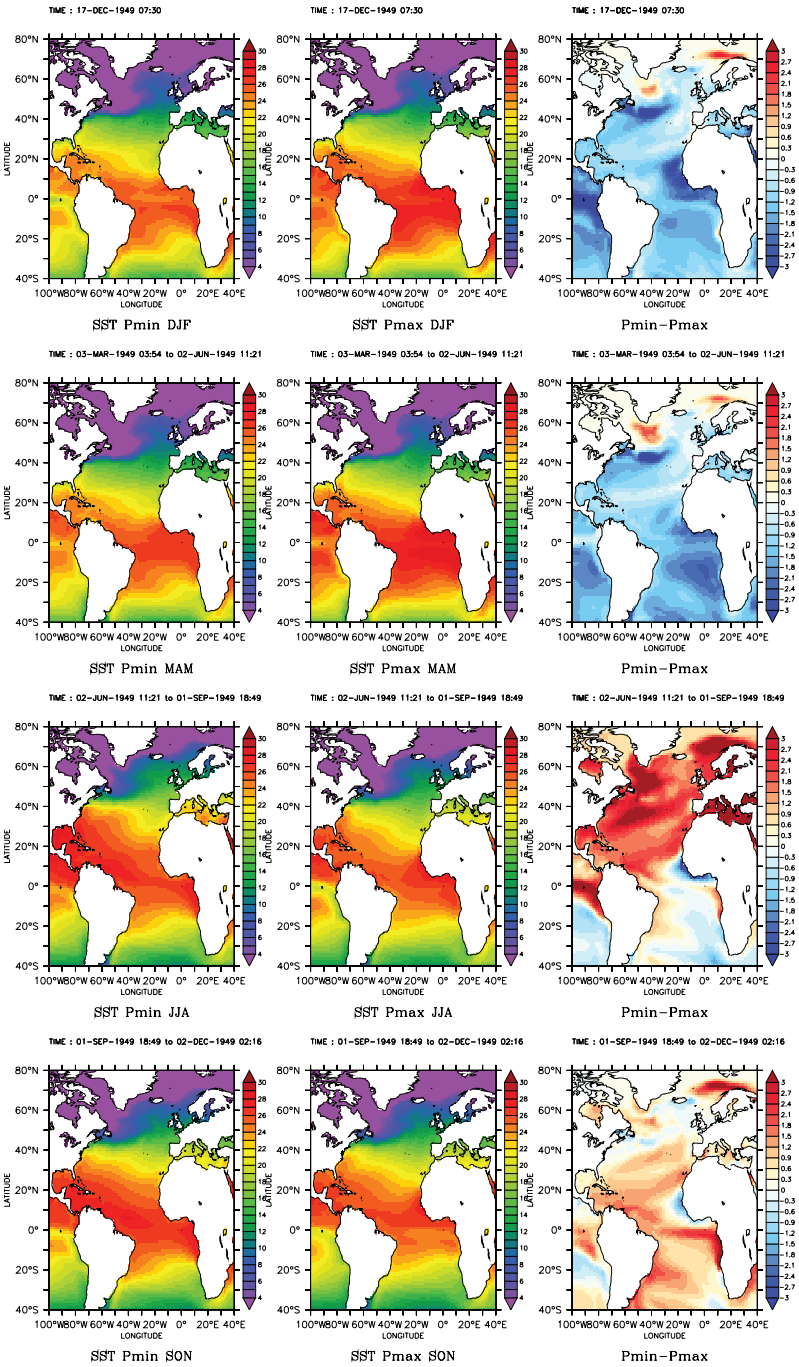

Figure S11. Sea surface temperature output of the model experiments of Bosmans, Drijfhout, et al. (2015). A high-resolution, coupled ocean-atmosphere, general circulation model was used. Experiments were performed with different astronomical parameters: minimum precession and minimum obliquity (Pmin), and maximum precession and minimum obliquity (Pmax). Outputs are shown for December to February (DJF), March to May (MAM), June to August (JJA), and September to November (SON).

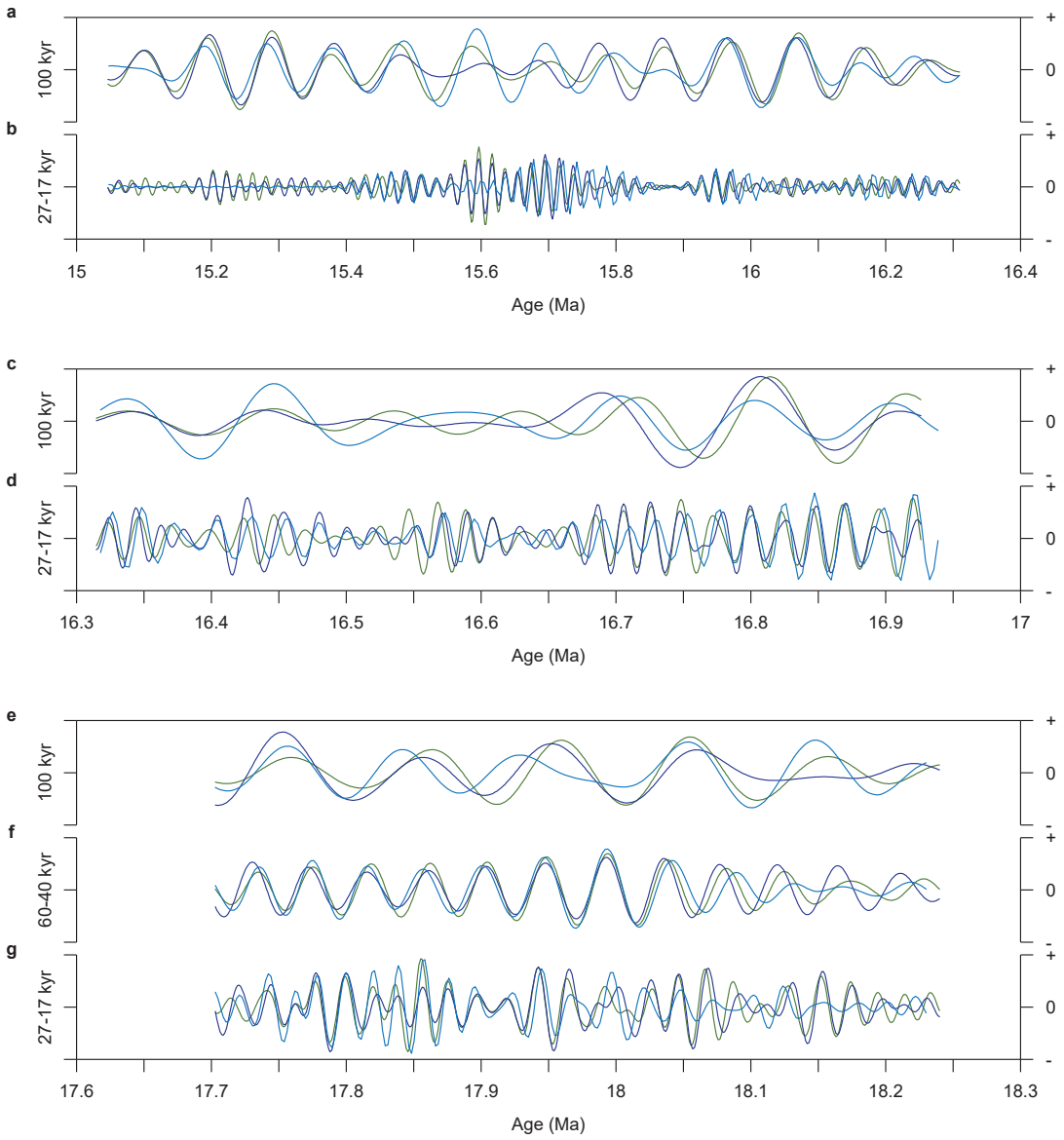

Figure S12. Phase relations between $\delta^{13}C$ (green), $\delta^{18}O$ (blue), and TEX_{86} (dark blue) on ~100 kyr, ~60-40 kyr, and ~27-17 kyr scales for three different intervals: 15.0-16.3 Ma (**a**), 16.3-16.9 Ma (**b**), and 17.7-18.2 Ma (**c**). See captions of Figures 6, 7, and 8 for bandpass filter widths.

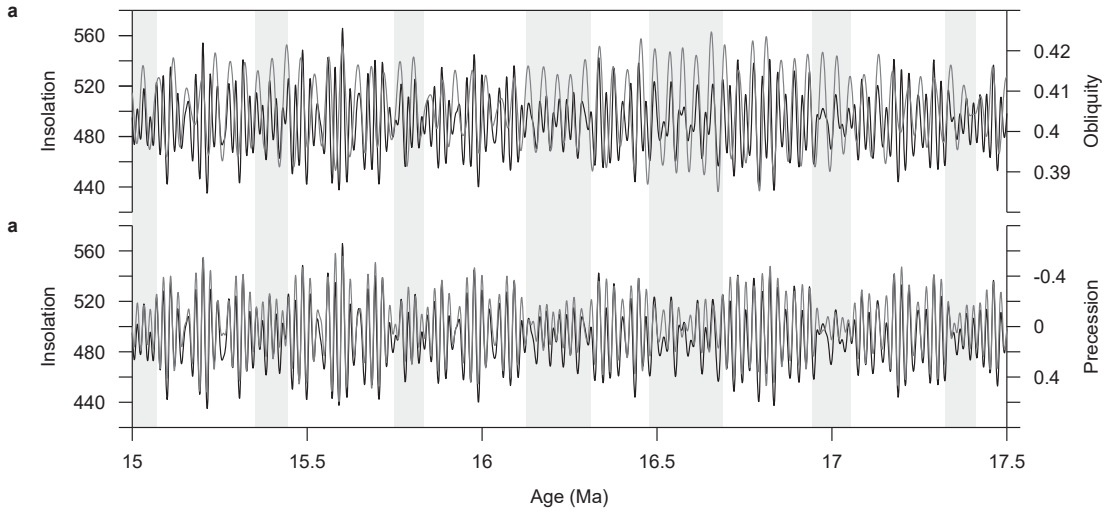

Figure S13. Summer (June 21) insolation at 65°N (black; **a-b**) compared to obliquity (grey; **a**) and precession (grey; **b**) of the La2004 solution (Laskar et al., 2004). Grey bars indicate 400 kyr eccentricity minima during which the amplitude of precession diminishes and obliquity becomes relatively more important in pacing insolation changes.

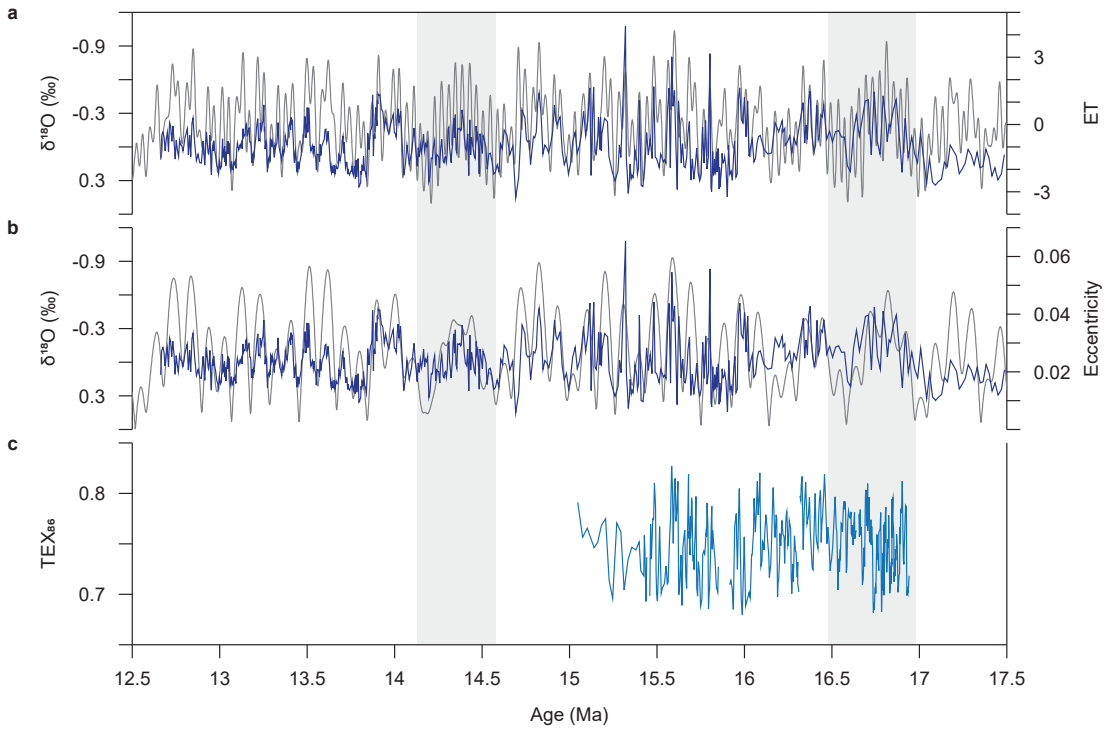

Figure S14. Comparison of the benthic $\delta^{18}O$ record of Site 1237 (Holbourn et al., 2007; **a-b**), the standardized eccentricity and tilt (ET) curve and eccentricity of La2004 (Laskar et al., 2004; **a-b**), and the TEX_{86} record of Site 959 (**c**). During 2.4 Myr eccentricity minima (grey bars) the dominant pacing switched from eccentricity to obliquity, which can be observed in the benthic $\delta^{18}O$ (see also Figure 3 of Holbourn et al., 2007) and TEX_{86} records (see also Figures 7 and 8). Note that the resolution of the benthic $\delta^{18}O$ record is lower in the interval before ~16.5 Ma.

Depth (rmbsf)	Age (Ma)
248.52	16.662
249	16.675
249.44	16.687
249.8	16.699
250.12	16.709
250.4	16.72
250.72	16.731
251.08	16.743
251.48	16.754
251.88	16.765
252.28	16.778
252.84	16.79
253.2	16.801
253.52	16.812
253.92	16.823
254.44	16.834
254.72	16.845
255.04	16.857
255.44	16.869
255.88	16.881
256.32	16.893
256.84	16.904
257.24	16.915

Table S1. Tie-points of the precession-based age model for core 25X. Tie-points are based on minima and maxima of the $\delta^{13}C$ bandpass filter in the depth domain (filter width of 0.63-1.75 1/m) and precession minima and maxima in the La2004 solution (Laskar et al., 2004; Figure S5).